NASA TECHNICAL NOTE

NASA TN D-2514




NASA TN D-2514

# STUDY OF WETTING AND NONWETTING MERCURY CONDENSING PRESSURE DROPS

*by Alfred Koestel, Martin U. Gutstein, and Robert T. Wainwright*

*Lewis Research Center*
*Cleveland, Ohio*

NATIONAL AERONAUTICS AND SPACE ADMINISTRATION • WASHINGTON, D. C. • NOVEMBER 1964

# STUDY OF WETTING AND NONWETTING MERCURY CONDENSING PRESSURE DROPS

By

Alfred Koestel
Thompson Ramo Wooldridge Inc.
Cleveland, Ohio

and

Martin U. Gutstein and Robert T. Wainwright
Lewis Research Center
Cleveland, Ohio

NATIONAL AERONAUTICS AND SPACE ADMINISTRATION

For sale by the Office of Technical Services, Department of Commerce,
Washington, D.C. 20230 -- Price $1.00

# STUDY OF WETTING AND NONWETTING MERCURY CONDENSING PRESSURE DROPS

by Alfred Koestel,* Martin U. Gutstein,
and Robert T. Wainwright

Lewis Research Center

## SUMMARY

Local static pressures were measured along tubes in which mercury vapor was flowing and condensing. The test sections consisted of constant-diameter tubes having inside diameters of 0.319 and 0.397 inch and a tapered tube of 0.4 to 0.2 inch inside diameter. The condensing lengths varied between 4 and 8 feet. The range of the mercury flow rates was 1.05 to 3 pounds per minute at inlet pressures of 8 to 30 pounds per square inch absolute.

The local two-phase frictional pressure drop data were obtained by assuming the average liquid velocity equal to the average vapor velocity at each location within a test section (i.e., a slip ratio of 1). A comparison of these data with the Lockhart-Martinelli correlation showed significant deviations, particularly at the low qualities. A relation between the local two-phase frictional pressure drop and the Weber number (based on the superficial vapor velocity), derived from fog-flow considerations, correlated the trend of the data over the full quality range. The derivation of this relation and a description of the flow regime on which it is based are presented. A similarity between the wetting and nonwetting frictional pressure drops for mercury condensation is likewise shown.

## INTRODUCTION

Rankine cycle powerplants utilizing mercury as a working fluid are being considered for space applications. Inherent in the performance of such plants is the need to condense the effluent of the turbine, that is, the mercury vapor. In a powerplant for space, this process might occur inside tubes, and the heat of condensation would be dissipated by radiation. To specify the dimensions of the tubes, their diameter, length, taper, etc. requires accurate prediction of the pressure drops associated with mercury condensing at low heat fluxes. In recognition that such predictions are not available, experiments were performed to measure the local static pressure along tubes of constant and

*Thompson Ramo Wooldridge Inc., Cleveland, Ohio.

varying diameter in both the wetting and nonwetting regimes. Moreover, an analysis of the fluid mechanics of condensing mercury was undertaken to develop a means to predict these pressure drops.

A veritable literature exists today that describes, predicts, and correlates two-phase frictional pressure gradients. For condensation, however, and for mercury condensation in particular, the correlation of Lockhart and Martinelli (ref. 1) and its refinement, the correlation of Baroczy and Sanders (ref. 2), are of most significance. The Lockhart-Martinelli approach consists of equating the pressure gradients obtained from adiabatic, two-component flows to the case of condensation at the equivalent liquid to vapor superficial pressure-gradient ratios. The total frictional pressure difference across a condenser tube may then be obtained by integration of the local gradients. The work of Baroczy and Sanders constituted an improvement to this correlation by accounting for a vapor Reynolds number effect that they observed in experiments with the adiabatic flow of mercury and nitrogen.

Hays (ref. 3) applied these correlations to mercury condensation data and found general agreement to within about ±25 percent. At low heat rejection rates or at low qualities (low vapor Reynolds numbers), however, Hays concluded that agreement of the test results with these correlations was not apparent. Hays attributed this finding to fog flow and believed the Lockhart-Martinelli correlation to be inapplicable to this flow regime.

Kiraly (ref. 4) presents a comparison of two-phase mercury-nitrogen pressure differences with the Martinelli curve. He likewise compares overall pressure differences of mercury condensation in horizontal tubes with the same correlation. In both cases agreement is good; however, condensation inside horizontal tapered tubes and inclined tubes of constant diameter showed considerable deviation. Thus it appears that the Lockhart-Martinelli correlation does not satisfactorily predict the pressure gradients of mercury condensation at low vapor velocities and low heat fluxes or those for unusual geometries and orientations. This conclusion implies that the pressure drops for mercury condensation should be distinguished from those obtained from adiabatic experiments.

The experimental data from this study were compared with Lockhart-Martinelli and significant deviations were likewise found, particularly at low qualities. The trends of the data, however, were predicted by an analysis of pressure differences based on the flow of a mixture of entrained drops and vapor through a passage formed by stationary wall-adhering drops. This particular fog-flow pattern may be for nonwetting fluids analogous to the spray-annular regime of wetting fluids to which the Lockhart-Martinelli correlation is known to be inapplicable (refs. 5 and 6). The pressure-drop data, which were obtained when the mercury seemingly wetted the tube wall, were also correlated by the fog-flow theory; the true flow regime for this mode of mercury condensation therefore remains uncertain. A discussion of these matters is presented herein.

The experimental and analytical efforts described in this article were performed at Thompson Ramo Wooldridge Inc. under NASA Contract NAS 3-2159. The authors are indebted to R. Gido and T. Jaenke, who built the equipment and performed the experiments.

## SYMBOLS

| | |
|---|---|
| $A$ | tube cross-sectional area, sq ft |
| $\overline{A}$ | tube average cross-sectional area defined by equation (C3), sq ft |
| $C_{d,\delta}$ | drag coefficient for mercury drops, dimensionless |
| $D$ | diameter, ft |
| $E_\sigma$ | constant of eq. (B1), dimensionless |
| $f$ | friction factor, dimensionless |
| $f$ | function of |
| $G$ | mass velocity, lb mass/(sec)(sq ft) |
| $g$ | local gravitational acceleration, ft/sec$^2$ |
| $g_c$ | conversion factor, 32.174 (lb mass)(ft)/(lb force)(sec$^2$) |
| $h_{fv}$ | heat of vaporization, Btu/lb mass |
| $L$ | length, ft |
| $M$ | mass flow rate, lb mass/sec |
| $n$ | ratio, $g/g_c$, lb force/lb mass |
| $P$ | pressure, lb force/sq ft |
| $Q$ | heat flux, Btu/(sec)(sq ft) |
| $R$ | volume fraction, dimensionless |
| Re | Reynolds number, dimensionless |
| t - t | Lockhart-Martinelli turbulent-liquid - turbulent-vapor flow regime |
| t - v | Lockhart-Martinelli turbulent-liquid - viscous-vapor flow regime |
| $U$ | average velocity, ft/sec |
| v - t | Lockhart-Martinelli viscous-liquid - turbulent-vapor flow regime |
| $x$ | quality, dimensionless |
| $\delta$ | drop diameter, ft |
| $\theta$ | angle of inclination, radians |
| $\mu$ | viscosity, lb mass/(ft)(sec) |
| $X$ | Lockhart-Martinelli parameter, dimensionless |

$\rho$ density, lb mass/cu ft

$\sigma$ surface tension, lb force/ft

$\Phi$ Lockhart-Martinelli modulus, dimensionless

Subscripts:

cr critical

D effective

f liquid

m fog mixture

mo momentum

s static

T total or tube

tpf two-phase frictional

v vapor

1 inlet of tube increment

2 exit of tube increment

## DESCRIPTION OF EQUIPMENT AND PROCEDURE

### Equipment

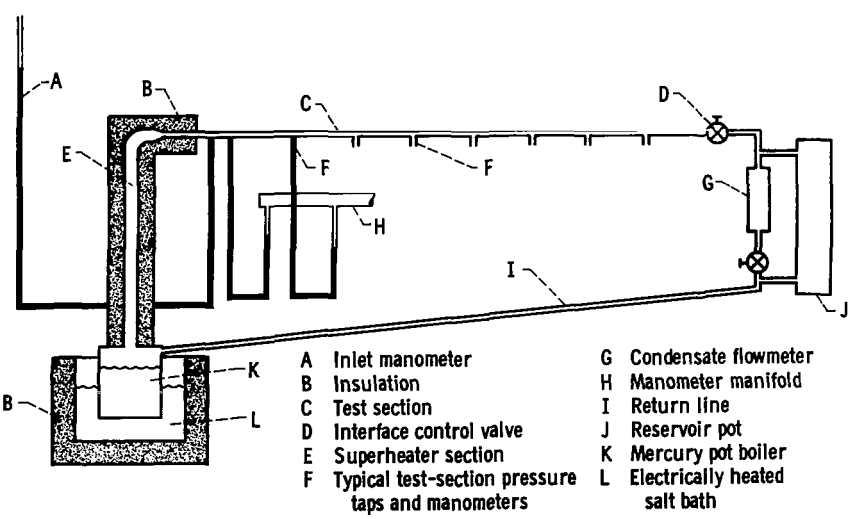


Figure 1. - Schematic drawing of mercury condensing test rig.

The mercury condensing experiments were conducted in a closed, natural circulation test loop shown schematically in figure 1. Fabricated entirely of stainless steel except for some of the condenser test sections, the rig consisted of a mercury pot boiler, a superheater section, and a flow-metering unit. Each condenser test-section tube was welded into the rig be-

tween the superheater and the flowmeter. Brief descriptions of these components are now presented.

The pot boiler consisted of an 8-inch-diameter by 9.75-inch-tall cylinder partly immersed in an electrically heated salt bath. A baffle-cup arrangement was provided at the top of the boiler (at the entrance to the superheater) to separate and recirculate any liquid mercury entrained in the vapor. The salt-bath heaters were capable of generating a maximum of 9 kilowatts of heat at bath temperatures up to about 1000° F.

The superheater was an electrically heated L-shaped tube that extended from the top of the boiler to the inlet of the test section. The vertical portion was 4 feet long and 1 inch in diameter, and the horizontal portion was 1 foot long. The inner diameter of the horizontal portion was machined to match the inlet internal diameter of each test section, thereby minimizing flow disturbances. The electric heater that was wrapped entirely about this component of the rig was capable of generating 4.5 kilowatts of heat and was employed to superheat the vapor slightly. Thus, any entrained liquid that managed to enter the superheater was probably vaporized.

Four condenser test sections, including both constant diameter and tapered tubes, were employed in this investigation. Their geometry and materials of construction are described in table I. The range of such experimental variables as the flow rate, the inlet pressure, the inlet vapor velocity, etc. is likewise listed in the table. Static-pressure taps at intervals of 14 to 18 inches along the tube length were provided for each test section. These taps consisted of lengths of stainless-steel tubing, 0.085-inch inner diameter, connected directly to stainless-steel mercury manometers. The low-pressure sides of the manometers were made of transparent plastic tubing. One of these manometers measured the static pressure at the test-section inlet relative to atmospheric pressure. The remaining manometers were connected to a common manifold and were used to measure relative static pressures.

Each test section was cooled by a crossflow of air from two diametrically opposed plenums. Because the air heat-transfer coefficient was controlling, the heat flux was essentially constant over the full length of the tube. A maximum heat flux of about 40,000 Btu per hour per square foot was attainable.

The principal features of the condensing process that occurred inside the test sections were observed with an X-ray unit and fluoroscope screen. This combination was mounted on a track and could traverse the entire test-section length. It was also employed to check the mercury level in the manometer taps at the junction to the test section and to detect the presence of large quantities of noncondensible gases downstream of the interface.

The mercury flow rate was measured by timing the collection of a known volume of condensate in a glass vessel located between the test section and the boiler. Care was taken to preserve the steady-state condition of the rig during a flow measurement.

## Operation

Prior to startup, the levels of mercury and molten salt were carefully adjusted to ensure a steady boiling process. Previous experience with the rig had shown that too low a salt level prevented the attainment of the higher vapor flow rates because of insufficient boiler heat-transfer area. Too high a mercury level often caused severe pressure oscillations.

At startup the manometer lines were closed and the rig was evacuated. The salt bath heaters were then energized and the flow of cooling air was initiated. Once a steady flow of mercury vapor was obtained, the manometers were opened. Noncondensible gases were continuously removed by a vacuum pump until X-ray examination of the interface no longer indicated their presence. Thereafter the tube wall temperature immediately upstream of the interface was used to monitor the presence of noncondensible gases. Whenever this temperature was well below the average condenser wall temperature, it indicated the collection of these gases at this location.

Data were recorded after attaining a steady-state condition that was defined by the constancy, for a period of at least 15 minutes, of the manometer levels, the boiler, the salt-bath and wall temperatures, and the vapor-liquid interface position.

## ANALYSIS OF EXPERIMENTAL DATA

The pressure, flow-rate, and condensing-length data obtained in this investigation are presented in table II.

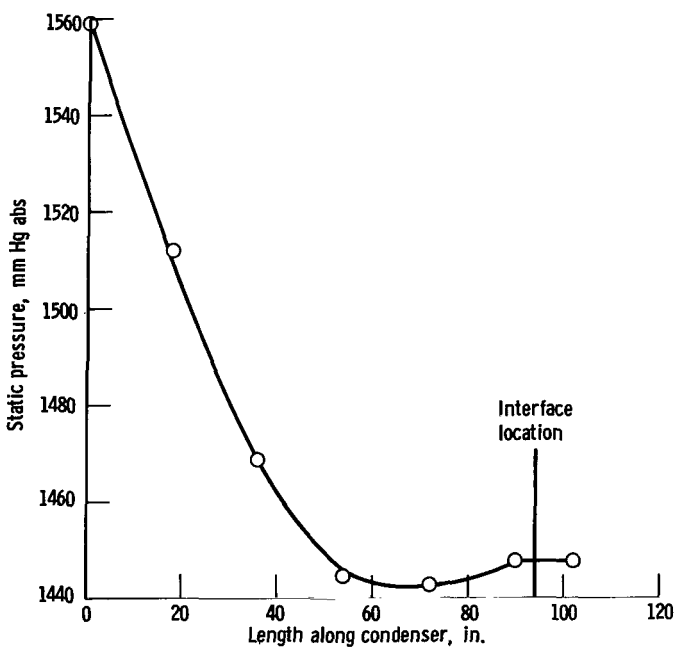


Figure 2. - Typical static-pressure profile. Run A-44.

Figure 2 illustrates a typical static-pressure profile along the test section. The rise or recovery of the static pressure toward the outlet of the test section is characteristic of condensing and is attributable to the effect of net momentum changes. These momentum changes have to be estimated in order to obtain the two-phase frictional pressure drops. A description of the method used to calculate the momentum changes is now presented.

The static-pressure difference measured between two taps of a horizontal constant-diameter tube in which condensing occurs is given by the expression

$$-dP_s = dP_{tpf} + dP_{mo} \qquad (1)$$

It can be shown that the $dP_{mo}$ term can be expanded to give

$$-dP_s = dP_{tpf} + \frac{G_T^2}{g_c}\left\{d\left[\frac{(1 - x)^2}{\rho_f R_f}\right] + d\left(\frac{x^2}{\rho_v R_v}\right)\right\} \qquad (2)$$

Equation (2) indicates that the frictional component of the static-pressure difference can be obtained only when the volume fractions or local slip ratios $U_f/U_v$ are known. The slip ratio is related to the volume fraction by

$$R_v = \frac{1}{\frac{1 - x}{x}\frac{\rho_v}{\rho_f}\frac{U_v}{U_f} + 1}$$

(It should be noted that $R_f$ does not include the stationary liquid drops at the wall. Experimental measurements of $R_f$ must therefore distinguish between the moving and the stationary liquid.)

Presently, the only correlation of mercury volume fractions available is that derived from adiabatic nitrogen-mercury measurements as reported by Baroczy (ref. 7). This correlation is believed inapplicable to mercury condensing. Hays (ref. 3) reported frictional pressure gradients of condensing mercury for two limiting cases, those of slip ratios of 0 and 1. Hays further recommended a slip of zero based on photographic evidence and the agreement of his data with the Lockhart-Martinelli correlation. As mentioned previously, however, deviations from this correlation were noted, particularly at low heat fluxes. These deviations were attributed to the presence of fog flow (i.e., slip ratios of approx. 1).

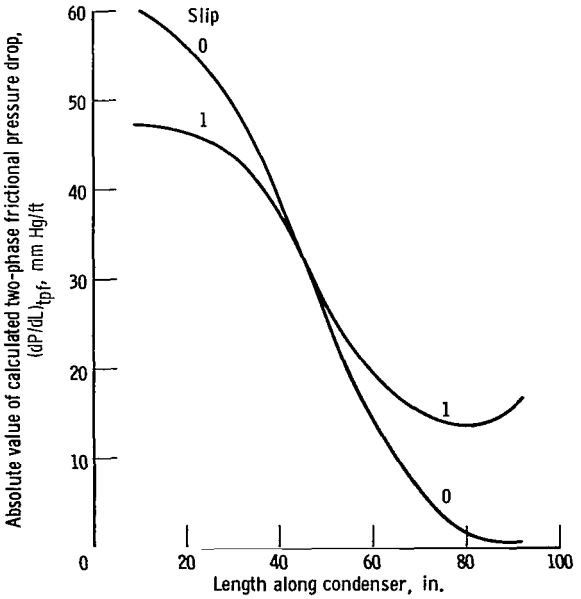


Figure 3. - Calculated values of two-phase frictional pressure gradients as function of condenser length for slip ratios of zero and one. Run A-44.

Figure 3 presents the frictional pressure gradients obtained from the data of figure 2, calculated on the basis of slip ratios of both 0 and 1. Significantly different gradients can clearly be obtained depending on the slip value chosen.

The authors of this report assumed a slip ratio value of 1 to obtain the frictional pressure gradients from their experimental data. This assumption was supported by the following evidence: Observations of the condensing process by means of the X-ray indicated that the predominant flow regime for low-heat-flux mercury condensation appeared to be that of a dispersion of fine drops flowing with the vapor, which is frequently called fog

flow. The assumption of a slip ratio of 1 for this regime is considered reasonable. Furthermore, an analysis was performed to predict the velocity and position of mercury drops entrained and flowing in a vapor stream. Figure 4 shows a typical result of this analysis. The velocity of drops entrained at positions corresponding to the inlet and 0.2, 0.4, 0.6, and 0.8 of the condensing length are plotted along with the vapor velocity distribution. This figure indicates that most drops are rapidly accelerated to very nearly the local gas velocity, and that the drops then follow this velocity even though it diminishes because of condensation. Only drops entrained near the interface, such as at the position corresponding to 0.8 of the condensing length, do not possess a slip ratio approximating 1. Even so, the drops that were entrained upstream of this position and that constitute the bulk of the liquid phase in the vapor at this position all possess slip ratios very nearly equal to 1. Finally, the assumption of a slip ratio of 1 was borne out by the general correlation of the frictional-pressure-drop data with the fog-flow analysis presented in appendix B. A discussion of this correlation is presented in the section FOG-FLOW CORRELATION OF NONWETTING DATA.

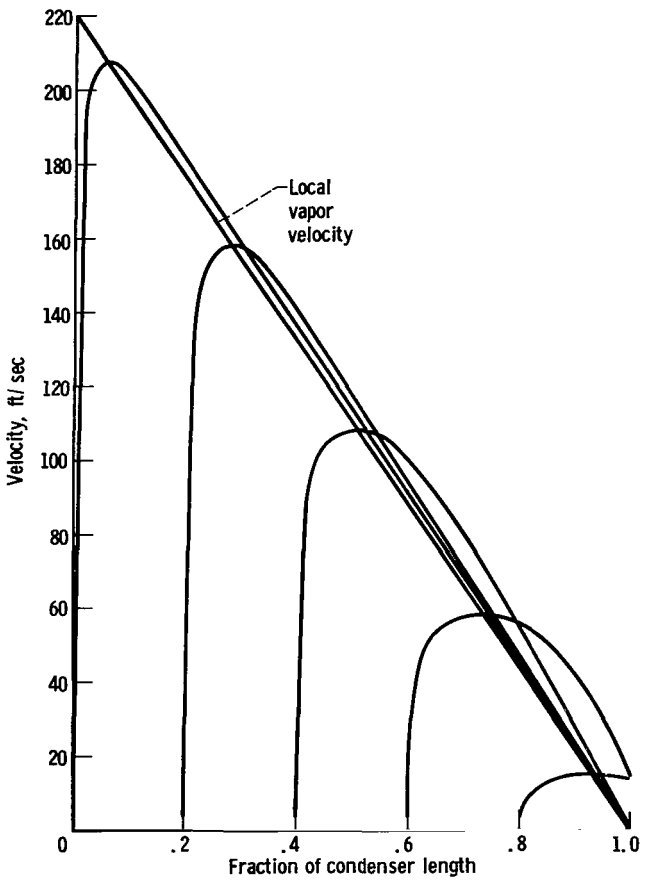


Figure 4. - Computed local vapor velocity and velocity of mercury drops entrained at various positions along condenser length.

## DISCUSSION OF RESULTS

### Empirical Correlation of Nonwetting Data

A correlation of adiabatic, two-component, two-phase frictional pressure drops was proposed by Lockhart and Martinelli (ref. 1). This frequently cited correlation presented a relation between the parameters $\Phi_v^2$ and $X$ defined as follows:

$$\Phi_v^2 = \frac{(\Delta P/\Delta L)_{tpf}}{(\Delta P/\Delta L)_v}$$

$$X = \sqrt{\frac{(\Delta P/\Delta L)_f}{(\Delta P/\Delta L)_v}}$$

Four flow regimes were also distinguished in accordance with the values of the superficial Reynolds numbers of the phases. Of these, only the viscous liquid - viscous vapor regime was not encountered in the mercury condensing experiments.

Figure 5 presents the Lockhart-Martinelli curves and the data of Series F, typical of the nonwetting condensing experiments. Examination of this figure shows that the Lockhart-Martinelli correlation appears to predict the data only at the high-quality region (i.e., low values of X). At low qualities the data deviate considerably from the correlation; furthermore, the data do not seem to segregate by flow regime in the manner suggested by Lockhart-Martinelli.

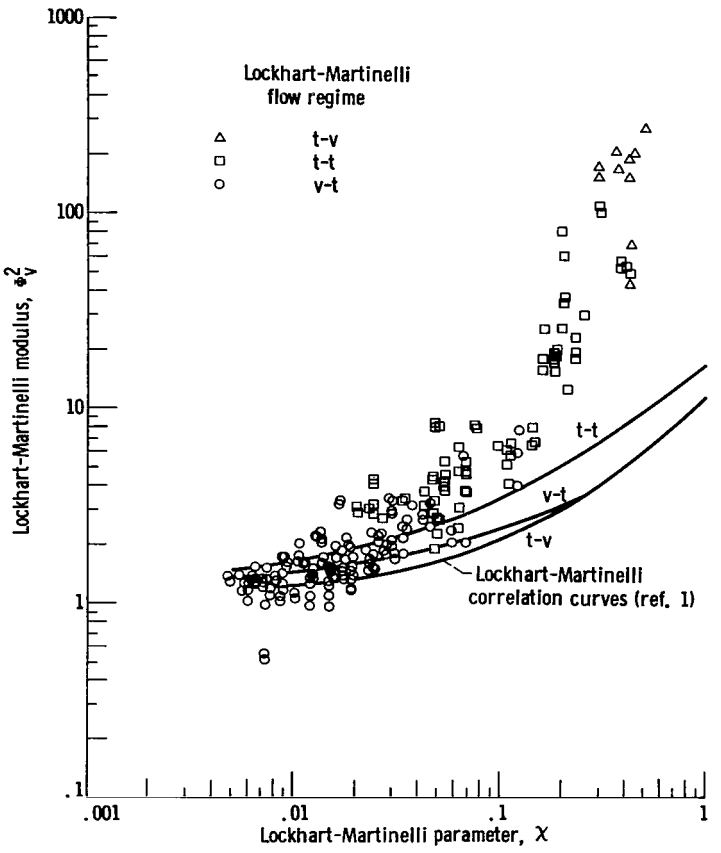


Figure 5. - Comparison of nonwetting data of Series F with Lockhart-Martinelli correlation.

The modified version of the Lockhart-Martinelli correlation of reference 2 likewise did not correlate the mercury-condensing data. In general, the experimentally determined pressure drops were larger than the predicted ones, and a clear vapor Reynolds number effect could not be established. A similar conclusion was drawn in reference 3.

## Fog-Flow Correlation of Nonwetting Data

Appendix A presents a detailed description of the fog-flow regime believed to be predominant in nonwetting mercury condensation. This description forms the basis of the theory that is derived in appendix B. A brief summary of both the flow model and the analysis is presented as well as a comparison of predicted and experimentally determined pressure drops.

X-ray examination of the condenser test sections indicated that, for nonwetting condensing, drops are formed at the heat-transfer surface and grow until they are displaced and entrained into the vapor stream. The mixture of entrained drops and vapor therefore flows through a passage formed by the sta-

tionary wall-adhering drops. The diameter of this passage $D_m$ is less than the tube diameter $D_T$ by twice the thickness of the drop layer. Application of the Fanning equation for frictional pressure drop due to a homogeneous or fog-flow dispersion gave the following result in terms of the Lockhart-Martinelli modulus $\Phi_v^2$, the quality, and the ratio of the diameters:

$$\Phi_v^2 x^{3/4} = \left(\frac{D_T}{D_m}\right)^{4.75} \tag{B11}$$

Likewise, by assuming the drop layer thickness to be equal to the diameter of drops at incipient entrainment, a relation was derived between the Weber number (based on the superficial vapor velocity) and the ratio of the diameters:

$$\frac{D_T \rho_v U_v^2}{2 g_c \sigma} = \frac{0.371}{\left(\frac{D_T}{D_m}\right)^4 - \left(\frac{D_T}{D_m}\right)^3} \tag{B19}$$

The constant 0.371 was determined by experiments with single mercury drops on a flat inclined plate (see appendix B). Thus by selecting values of the ratio $D_T/D_m$, the relation between $\Phi_v^2 x^{3/4}$ and the local Weber number was obtained. This relation is plotted as the curves of figures 6 to 9. The experimental

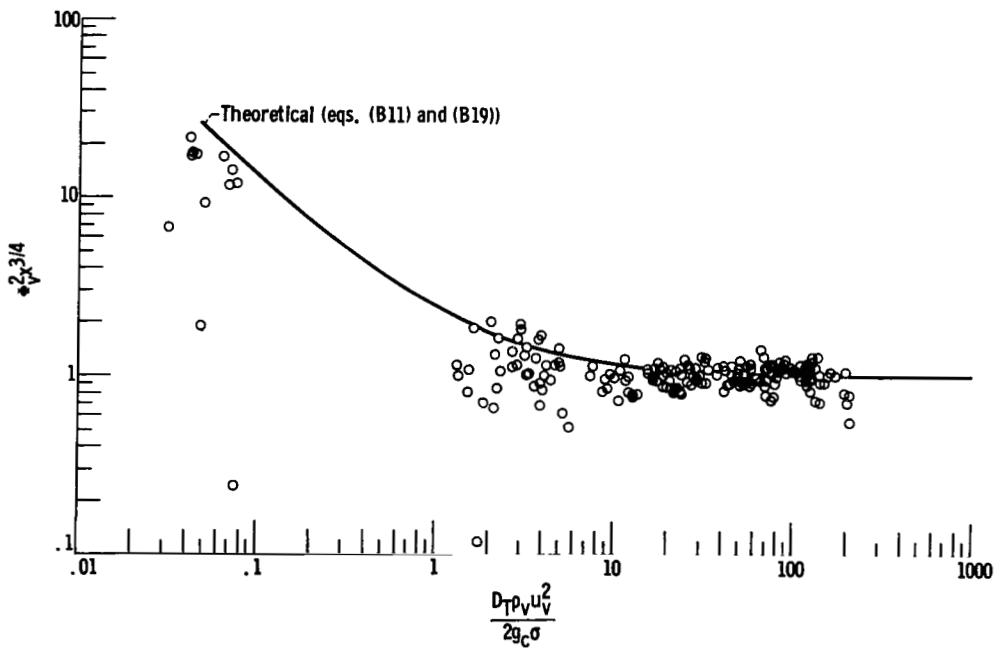


Figure 6. - Comparison of Series A data with fog-flow prediction.

values of these parameters are also plotted in these graphs for confirmation of the fog-flow theory. The calculation of the parameters $\Phi_v^2 x^{3/4}$ and the Weber

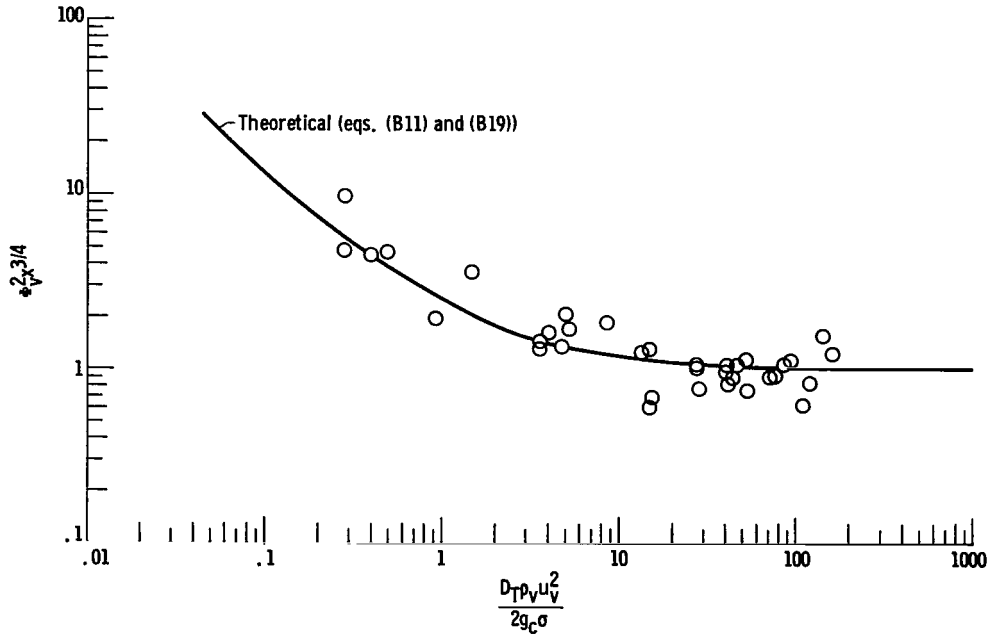


Figure 7. - Comparison of Series D data with fog-flow prediction.

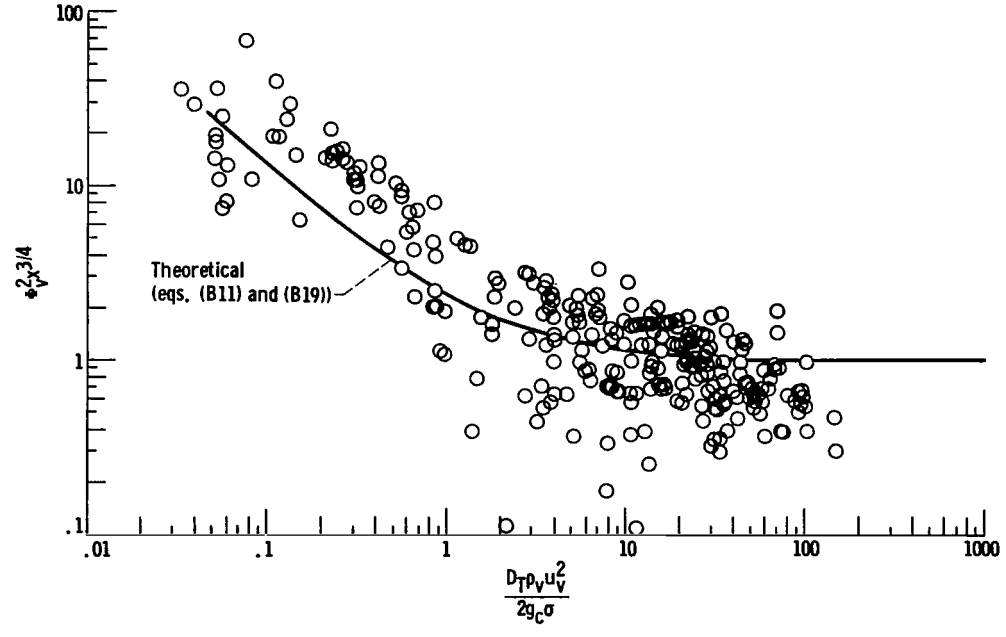


Figure 8. - Comparison of Series E data with fog-flow prediction.

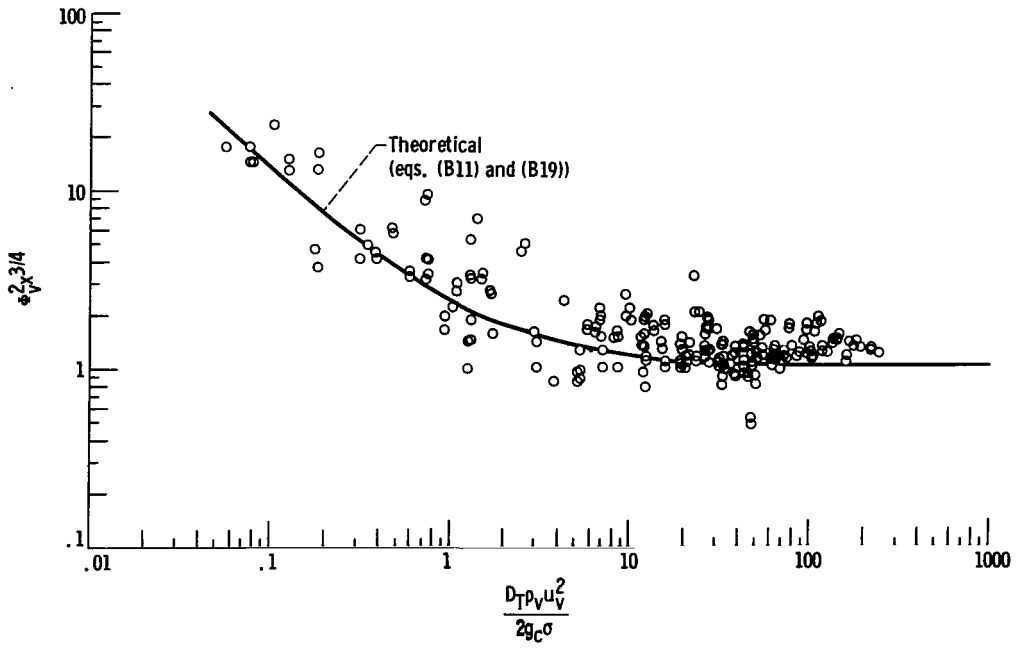


Figure 9. - Comparison of Series F data with fog-flow prediction.

number is illustrated in appendix C for the tapered test section.

Figures 6 to 9 compare the pressure-drop data of Series A, D, E, and F, respectively, with the fog-flow theory (see table I). These figures show that, at Weber numbers greater than about 10, the experimental values of $\Phi_v^2 x^{3/4}$ seem to equal 1 and are independent of the Weber number (i.e., the thickness of the drop layer is very nearly negligible). At lower values of the Weber number, $\Phi_v^2 x^{3/4}$ becomes significantly greater than 1 and dependent on the Weber number. Although considerable scatter is present, the fog-flow theory predicted this trend of the data. The greater scatter of the data for the Series E tests was attributed to the larger tube diameter and the consequent difficulty in measuring the smaller frictional pressure drops or to a deviation from fog-flow due to the lower vapor velocities.

## CORRELATION OF WETTING DATA

Prolonged testing with the constant-diameter tube of Series A caused the mercury to wet the condensing surface. The data that were recorded during this condition were reported as the Series W experiments. To explore this phenomenon in greater detail, the Series G tests were performed with magnesium and titanium added to the mercury to induce wetting. Both the Series W and G experiments were characterized by elongated interfaces, as shown in figure 10, as opposed to the more or less vertical interfaces present in the nonwetting tests.

Figure 11 presents the Series G data plotted in accordance with the Lockhart-Martinelli correlation. Comparison of this figure with figure 5

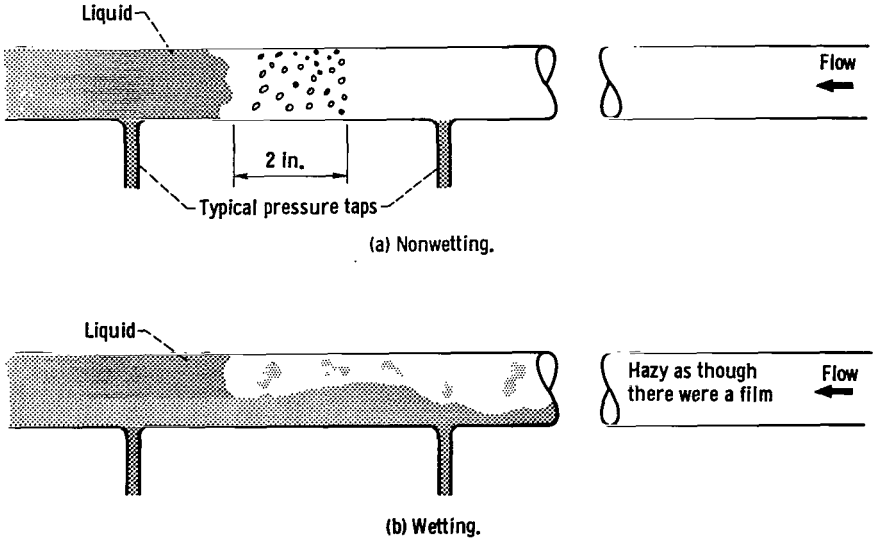


Figure 10. - Schematics of fluoroscopic observations during condensation of mercury in horizontal 316 stainless-steel tube.

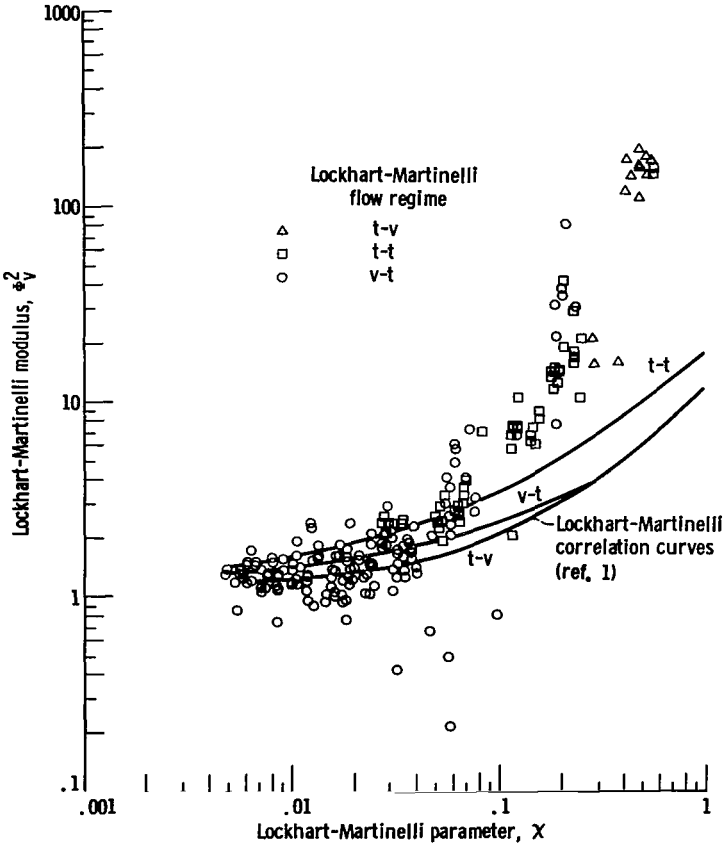


Figure 11. - Comparison of wetting data of Series G with Lockhart-Martinelli correlation.

illustrates an unusual similarity between the wetting and nonwetting two-phase frictional pressure differences. This similarity is further indicated by figures 12 and 13 in which the Series W and G data are correlated with the fog-flow parameters. That the fog-flow theory predicts the pressure-drop trends for the wetting condensation is probably explained by one of the following two possibilities: The degree of wetting induced by the additives may have been limited and the condensation may still have been essentially dropwise, or, on the other hand, wetting may actually have been the mode of condensation. If the latter were true, the results of figures 12 and 13 would indicate that the fog regime was still present, but a liquid film rather than a drop layer covered the inner surface of the

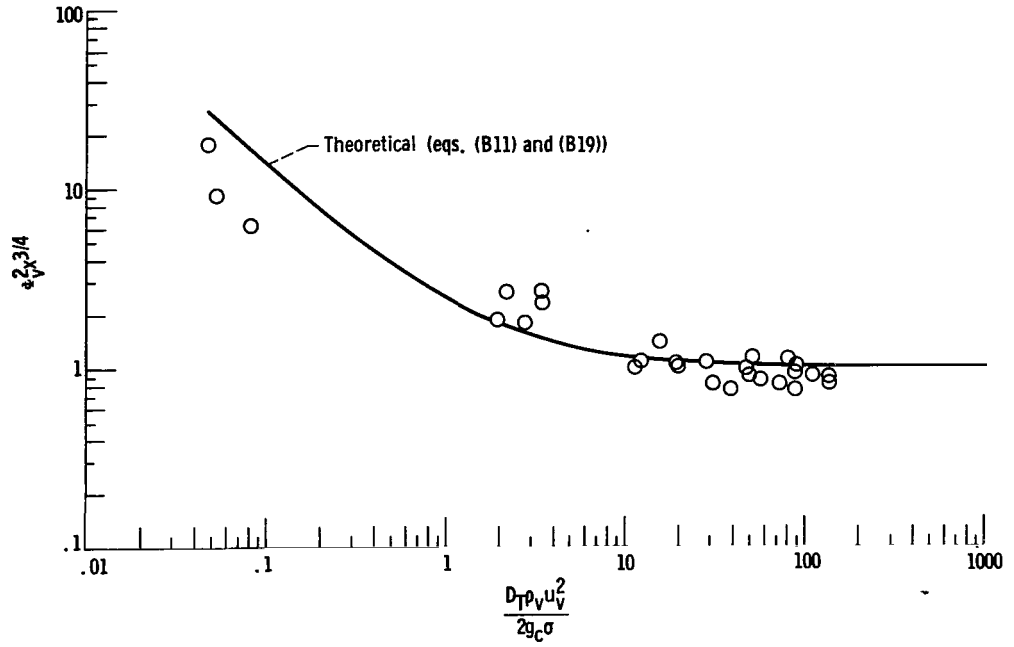


Figure 12. - Comparison of Series W data with fog-flow prediction.

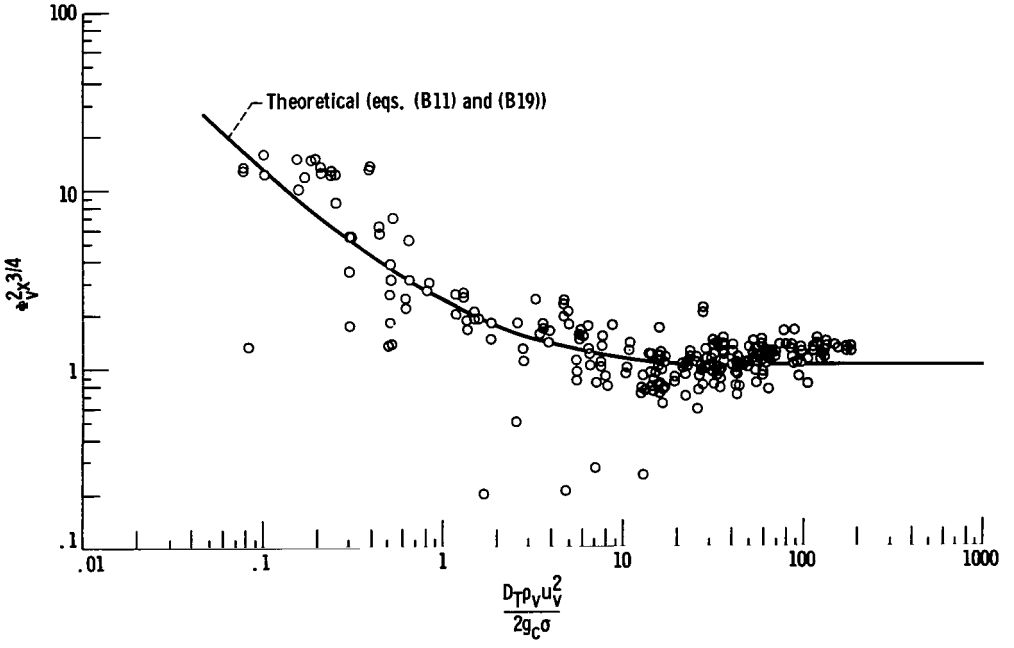


Figure 13. - Comparison of Series G data with fog-flow prediction.

tube (i.e., spray-annular flow regime). Moreover, this film must have behaved very much like the drop layer; that is, the thickness of the layer and its surface roughness had to be comparable, and the drops entrained from the film had to be similar in number and size at incipient entrainment to the nonwetting entrained drops. Koestel and Smith (ref. 8) analyzed the spray-annular flow regime and, by application of film-stability considerations, likewise achieved correlation of the Series G data. Thus, further experimental work and analyses are required to determine which of these flow models, the fog-flow regime with stationary wall drops or the spray-annular film regime, more accurately describes the flow pattern for wetting mercury condensation.

## SUMMARY AND RECOMMENDATIONS

The experimental equipment used to measure local static-pressure drops for low-heat-flux mercury condensation was described. The frictional pressure drops that were obtained were shown to be inadequately predicted by the Lockhart-Martinelli correlation, particularly at low qualities. A fog-flow theory was formulated that was inferred from observations of the flow regime. A relation was obtained between the Weber number (based on the superficial vapor velocity) and the fog-flow parameter $\Phi_V^2 x^{3/4}$. Comparison of condensing mercury data obtained by the authors with this fog-flow relation showed that the theory satisfactorily predicted the trends of these data over a wide range of test conditions.

The authors recommend that future studies of mercury condensation determine the limits of the fog-flow theory since the application of the theory to condensation at higher heat fluxes and to the situation of wetting fluids is as yet uncertain. Finally, future investigations should include a study of the flow regimes encountered and a careful determination of the liquid volume fractions, both of which are essential to a complete understanding of the physics of condensation.

Lewis Research Center
National Aeronautics and Space Administration
Cleveland, Ohio, July 28, 1964

## APPENDIX A

## DESCRIPTION OF FLOW REGIME

Fundamental to the prediction of two-phase pressure drop or heat transfer is a knowledge of the existing flow regime. For condensation occurring inside tubes, wetting fluids generally form a thin annular layer at the heat-transfer surface. In all likelihood, drops are sometimes broken from this film and entrained in the vapor core. For mercury condensation, however, a continuous liquid film is difficult to obtain even when the mercury wets its container. More typically a layer of drops is formed at the tube wall. The greater portion of the condensate is then transported to the tube exit by the entrainment of these drops into the vapor stream. At relatively high vapor velocities this two-phase flow has been observed and described as a fog flow (ref. 9). Even at lower vapor flow rates the fog regime is probably present although gravity effects, such as large agglomerated drops, do appear. A more detailed picture of the fog-flow regime of mercury condensation is offered for the purpose of deriving a two-phase frictional-pressure-drop prediction.

The authors postulate that the drops entrained into the vapor stream are extremely small (of the order of 0.001 to 0.010 in. in diameter) and are rapidly accelerated to very nearly the local vapor velocity. The drops are further conceived to respond to the turbulent fluctuations of the vapor phase and are dispersed so that the effects of concentration gradients are negligible. In effect, the drops travel with and become part of the vapor stream; the two-phase mixture is thus assumed to behave as a single-phase fluid.

This liquid-vapor fog flows through the passage formed by the drops that are attached to the tube wall. The passage, however, is essentially hydraulically smooth because of the close packing of the drops on the wall. It is further assumed that increasing the packing of the drops at the wall by raising the heat flux would have little or no effect on the friction factor. The diameter of the duct through which the fog-like mixture flows is $D_T - 2\delta_D$, where $\delta_D$ is the effective thickness of the drop layer at a particular location.

In a previous study performed by Denington, et al. (ref. 10) it was shown that the diameter of the mercury drops entrained into a flowing nitrogen stream was related to the velocity of the gas. It is suggested that such a relation also exists for mercury condensing: a drop grows to a particular size called the critical drop diameter (defined by the velocity of the vapor) and is then entrained into the vapor core. The effective thickness of the drop layer on the wall at a particular position was therefore taken as equal to the critical drop diameter at that position. Thus, the vapor velocity (here, the velocity of the fog) determines the thickness of the condensate layer at the wall and is, in turn, dependent on this thickness by continuity. The prediction of the frictional pressure gradients for condensing mercury based on the previous considerations is given in appendix B.

## APPENDIX B

## DERIVATION OF FOG-FLOW THEORY

### Critical Drop Size

Reference 10 presents a detailed experimental and theoretical analysis of the entrainment of mercury drops. A brief review of this work as it applies to mercury condensation is presented here, since the mechanics of this process forms an important part of the fog-flow model.

As a drop forms and grows on a tube surface, forces are produced that tend either to make the drop move or to oppose its movement. These forces consist of the drag caused by the flowing vapor, the gravity force, and the interfacial force between the drop and the wall arising from the deformation of the drop by either of the two previous forces. At a particular drop size, the critical drop diameter $\delta_{cr}$, these forces are no longer balanced and the drop is displaced. Thus, at incipient movement, the following force balance must be applicable:

$$\text{Drag Force} \pm \text{Gravity Force} - \text{Interfacial Force} = 0$$

or

$$\frac{\pi\delta_{cr}^2}{4} \frac{C_{d,\delta}\rho_v U_v^2}{2g_c} \pm n(\sin\theta)\rho_f \frac{\pi\delta_{cr}^3}{6} - \pi\delta_{cr}\sigma E_\sigma = 0 \tag{B1}$$

The coefficient of drag for drops $C_{d,\delta}$ is also dependent on the deformation. In general, the coefficients for deformable bodies (bubbles, drops, etc.) are greater than for solid spheres and have values very nearly equal to 1 (ref. 11). For simplicity, the coefficients may be assumed equal to 1 and the value of $E_\sigma$ can be made to accommodate the deformation effect. Thus, in horizontal tubes or in the absence of a gravitational field, the critical drop size is related to the vapor velocity as follows:

$$\frac{\delta_{cr}\rho_v U_v^2}{2g_c\sigma} = 4E_\sigma \tag{B2}$$

The term on the left side of equation (B2) is the Weber number for the drop. Through experiments conducted both in tubes and with inclined flat plates, $E_\sigma$ had the value of 0.0464. For a more detailed discussion of these experiments and their analysis, reference 10 should be consulted.

### Derivation of Fog-Flow Model

If the discussion of the previous sections truly describes the flow regime for mercury condensing inside tubes, then the frictional component of the

static pressure drop may be written as a single equation for both phases as follows:

$$\left(\frac{dP}{dL}\right)_{tpf} = \frac{f_m M_m^2}{2g_c D_m \rho_m \left(\frac{\pi}{4} D_m^2\right)^2} \tag{B3}$$

where

$f_m$ friction factor for fog mixture

$D_m$ diameter of flow passage formed by drops on wall through which fog flows

The frictional pressure drop that would result if the vapor portion of the fog were to flow through the bare pipe is

$$\left(\frac{dP}{dL}\right)_v = \frac{f_v (xM_m)^2}{2g_c D_T \rho_v \left(\frac{\pi}{4} D_T^2\right)^2} \tag{B4}$$

The Lockhart-Martinelli modulus $\Phi_v^2$, defined as the ratio of the two gradients, is therefore

$$\Phi_v^2 = \frac{f_m}{f_v} \frac{1}{x^2} \frac{\rho_v}{\rho_m} \left(\frac{D_T}{D_m}\right)^5 \tag{B5}$$

The friction factor for turbulent flow in smooth passages is given by

$$f_m = \frac{0.316}{Re_m^{0.25}} = \frac{0.316}{\left(\frac{4M_m}{\pi D_m \mu_m}\right)^{0.25}} \tag{B6}$$

and

$$f_v = \frac{0.316}{Re_v^{0.25}} = \frac{0.316}{\left(\frac{4xM_m}{\pi D_T \mu_v}\right)^{0.25}} \tag{B7}$$

The viscosities $\mu_m$ and $\mu_v$ are transport properties and are more dependent on the volume fraction of the two phases than on the weight fraction. Since the volume fraction of the flowing liquid is much less than 1, it can be assumed that

$$\mu_m = \mu_v \tag{B8}$$

(A similar assumption concerning the viscosities was made by Bankoff (ref. 12).) Therefore,

$$\frac{f_m}{f_v} = \left(\frac{D_m x}{D_T}\right)^{0.25} \tag{B9}$$

The density ratio may be considered to be weight fraction dependent. Thus,

$$\frac{\rho_v}{\rho_m} = x \tag{B10}$$

Combining equations (B5), (B9), and (B10) gives

$$\Phi_v^2 = \frac{1}{x^{3/4}} \left(\frac{D_T}{D_m}\right)^{4.75} \tag{B11}$$

A relation between $D_T/D_m$ and the Weber number may be derived for horizontal flow or zero gravity as follows: From equation (B2) the Weber number based on the tube diameter may be obtained:

$$\frac{D_T \rho_v U_m^2}{2 g_c \sigma} = \frac{4 E_\sigma D_T}{\delta_{cr}} \tag{B12}$$

Note that the vapor density is employed rather than the mixture density since only the vapor conditions influence the entrainment of a single drop.

From continuity,

$$\frac{\pi D_T^2}{4} \rho_v U_v = \frac{\pi D_m^2}{4} \rho_v U_m \tag{B13}$$

where $U_v$ represents the velocity of the vapor in a bare tube with all the liquid removed. Therefore,

$$\left(\frac{D_T}{D_m}\right)^2 U_v = U_m \tag{B14}$$

Substituting equation (B14) into (B12) yields

$$\frac{D_T \rho_v \left(\frac{D_T}{D_m}\right)^4 U_v^2}{2 g_c \sigma} = \frac{4 E_\sigma D_T}{\delta_{cr}} \tag{B15}$$

When the assumption that, at a particular point in the tube, the critical drop diameter corresponds to the effective thickness of the drop layer is utilized,

$$D_T - 2\delta_{cr} = D_m \tag{B16}$$

or

$$\frac{D_T}{\delta_{cr}} = \frac{2}{1 - \frac{D_m}{D_T}} \tag{B17}$$

Substituting equation (B17) into (B15) yields

$$\frac{D_T \rho_v U_v^2}{2 g_c \sigma} = \frac{4E_\sigma}{\left(\frac{D_T}{D_m}\right)^4} \frac{2}{1 - \frac{D_m}{D_T}} \tag{B18}$$

or

$$\frac{D_T \rho_v U_v^2}{2 g_c \sigma} = \frac{8E_\sigma}{\left(\frac{D_T}{D_m}\right)^4 - \left(\frac{D_T}{D_m}\right)^3} \tag{B19}$$

Thus from equations (B11) and (B19), a relation has been shown to exist between the Lockhart-Martinelli modulus $\Phi_v^2$ and the Weber number such that

$$\Phi_v^2 X^{3/4} = f\left(\frac{D_T \rho_v U_v^2}{2 g_c \sigma}\right) \tag{B20}$$

By assuming values of the ratio $D_T/D_m$, the relation between the Weber number and $\Phi_v^2 X^{3/4}$ may be obtained.

## Note on Derivation of Fog-Flow Model

Equation (B3) of the derivation assumes a homogeneous flow or a fog flow. An entirely similar expression was used by Owens (ref. 13) in calculating the pressure drops for air-water and steam-water mixtures. Comparison of his predictions with the Martinelli-Nelson correlation (ref. 14) gave reasonable agreement. Inasmuch as the Martinelli-Nelson correlation was based on Lockhart-Martinelli, it is therefore likely that the latter will correlate the pressure drops of a fog flow that completely fills its passage, that is, in which there is no annular liquid layer. Such a condition is apparently approached in mercury condensation at Weber numbers greater than about 10, corresponding to values of $X$ of less than about 0.04. Figure 5 shows that the Lockhart-Martinelli correlation does indeed seem to predict the pressure drops of this flow regime for the Series F data.

## APPENDIX C

## SAMPLE CALCULATION OF FOG-FLOW PARAMETERS FOR TAPERED TUBE CASE

### Momentum Changes

With reference to figure 14, a force balance in the axial direction may be written for an increment of condenser length as follows:

$$P_{s,1}A_1 - P_{s,2}A_2 - \left(\frac{P_{s,1} + P_{s,2}}{2}\right)(A_1 - A_2) - \frac{M_{f,2}U_{f,2}}{g_c} - \frac{M_{v,2}U_{v,2}}{g_c} + \frac{M_{f,1}U_{f,1}}{g_c}$$

$$+ \frac{M_{v,1}U_{v,1}}{g_c} = \frac{\Delta P_{tpf}}{\Delta L}\int_{L_1}^{L_2} A_T \, dL \qquad (C1)$$

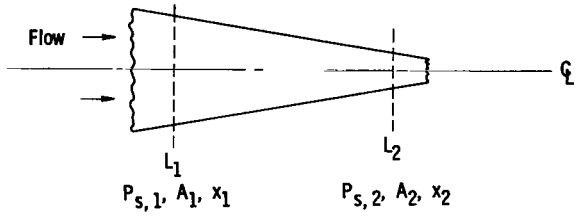


Figure 14. - Increment of tapered tube.

Equation (C1) assumes that the cross-sectional area changes are small relative to the tube length and that the two-phase frictional pressure drop varies little within the increment. By collecting terms and making the assumption that the slip equals 1 the following expression is obtained:

$$\frac{\Delta P_{tpf}}{\Delta L} = \frac{(P_{s,1} - P_{s,2})\bar{A} - \frac{M_T}{g_c}(U_{v,2} - U_{v,1})}{\int_{L_1}^{L_2} A_T \, dL} \qquad (C2)$$

where

$$\bar{A} = \frac{A_1 + A_2}{2} \qquad (C3)$$

Substituting for the vapor velocities yields

$$\frac{\Delta P_{tpf}}{\Delta L} = \frac{(P_{s,1} - P_{s,2})\bar{A} - \frac{M_T^2}{g_c}\left(\frac{x_2}{\rho_{v,2}A_{v,2}} - \frac{x_1}{\rho_{v,1}A_{v,1}}\right)}{\int_{L_1}^{L_2} A_T \, dL} \qquad (C4)$$

where

$$A_v = R_v A_T \tag{C5}$$

or

$$A_v = \frac{A_T}{\left(\frac{1 - x}{x}\right)\left(\frac{\rho_v}{\rho_f}\right) + 1} \tag{C6}$$

The quality at any point in the condenser tube is related to the heat flux Q by the expression

$$x = 1 - \frac{\pi}{M_T} \int_0^L \frac{Q\, D_T\, dL}{h_{fv}} \tag{C7}$$

Calculation of $\Phi_v^2 x^{3/4}$

The parameter $\Phi_v^2 x^{3/4}$ may be defined for an increment as follows:

$$\Phi_v^2 x^{3/4} = \frac{\frac{\Delta P_{tpf}}{\Delta L}}{\frac{\Delta P_v}{\Delta L}} \frac{\int_{L_1}^{L_2} x^{3/4}\, dL}{\Delta L} \tag{C8}$$

The term $\Delta P_v/\Delta L$ for the increment is calculated from the following expression:

$$\frac{\Delta P_v}{\Delta L} = \frac{8 M_T^2}{\pi^2 g_c\, \Delta L} \int_{L_1}^{L_2} \frac{x^2 f_v\, dL}{\rho_v\, D_T^5} \tag{C9}$$

The friction factor $f_v$ is given by

$$f_v = \frac{0.316}{\left(\frac{4 x M_T}{\pi\, D_T \mu_v}\right)^{0.25}} \tag{C10}$$

## Calculation of the Weber Number

The Weber number for the increment is obtained from the following expression:

$$\frac{D_T \rho_v U_v^2}{2 g_c \sigma} = \frac{M_T^2}{2 g_c \, \Delta L} \int_{L_1}^{L_2} \frac{D_T x^2 \, dL}{\sigma A_v^2 \rho_v} \qquad \text{(C11)}$$

## REFERENCES


1. Lockhart, R. W., and Martinelli, R. C.: Proposed Correlation of Data for Isothermal Two-Phase, Two-Component Flow in Pipes. Chemical Engineering Progress, vol. 45, no. 1, 1949, pp. 39-48.

2. Baroczy, C. J., and Sanders, V. D.: Pressure Drop for Flowing Vapors Condensing in a Straight Horizontal Tube. Atomics International Special Report, NAA-SR-6333, June 1961.

3. Hays, L.: Investigation of Condensers Applicable to Space Power Systems. Part I. Direct Condensers, Electro Optical Systems, Inc. Report 1588, Sept. 1962.

4. Kiraly, R., and Koestel, A.: The SNAP-2 Power Conversion System Topical Report No. 8, Condenser Development and Design Study. Thompson Ramo Wooldridge Inc. Report No. ER-4104, June 1960.

5. Hoogendoorn, C. J.: Gas-Liquid Flow in Horizontal Pipes. Chemical Eng. Science, vol. 9, no. 4, Feb. 1959, pp. 205-217.

6. Chien, S.: An Experimental Investigation of the Liquid Film Structure and Pressure Drop of Vertical, Downward, Annular, Two-Phase Flow. Ph.D. Dissertation, Univ. of Minnesota, April 1961.

7. Baroczy, C. J.: Correlation of Liquid Fraction in Two-Phase Flow with Application to Liquid Metals. Atomics International Special Report NAA-SR-8171, April 15, 1963.

8. Koestel, A., and Smith, C.: Radiator Design Limitations for Dynamic Converters. Paper Presented at Sixth AGARD Combustion and Prop. Colloquium, Cannes (France), Mar. 16-20, 1964.

9. Gido, R., and Koestel, A.: Mercury Wetting and Non-Wetting Condensing Research. Thompson Ramo Wooldridge Inc. Progress Report No. ER-5214, January 1963.

10. Denington, R. J., et al.: Space Radiator Study. Thompson Ramo Wooldridge Inc. Report ER-4544, April 30, 1962.

11. Hughes, R. R., and Gilliland, E. R.: The Mechanics of Drops. Chemical Engineering Progress, vol. 48, no. 10, October 1952, pp. 497-505.

12. Bankoff, S. G.: A Variable Density Single-Fluid Model for Two-Phase Flow with Particular Reference to Steam-Water Flow. Journal of Heat Transfer, Transaction of ASME, ser. C, vol. 82, 1960, pp. 265-272.

13. Owens, W. L., Jr.: Two-Phase Pressure Gradient. International Developments in Heat Transfer. Proc. 1961-1962 Heat Transfer Conference, ASME, 1963, pp. 382-390.

14. Martinelli, R. C., and Nelson, D. B.: Prediction of Pressure Drop During Forced-Circulation Boiling of Water. ASME, Trans., vol. 70, no. 6, August 1948, pp. 695-702.

TABLE I. - RANGE OF VARIABLES FOR MERCURY CONDENSING EXPERIMENTS

| Variable | Series A | Series D | Series E | Series F | Series G | Series W |
|---|---|---|---|---|---|---|
| Condensing length, in. | 94 | 48 - 82 | 48 - 95 | 53 - 94 | 53 - 94 | 94 |
| Tube inner diameter, in. | 0.319 | 0.4 × 0.2 | 0.397 | 0.319 | 0.319 | 0.319 |
| Tube material | 316 SS | Cobalt-base alloy[a] | Cobalt-base alloy[a] | Cobalt-base alloy[a] | Cobalt-base alloy[a] | 316 SS |
| Vapor inlet pressure, psia | 8.0 - 30.2 | 14.9 - 30.1 | 11.4 - 30.4 | 12.1 - 30.4 | 10.6 - 30.5 | 19.6 - 20.2 |
| Vapor inlet quality | 1.0 | 1.0 | 1.0 | 1.0 | 1.0 | 1.0 |
| Vapor inlet velocity, ft/sec | 114 - 278 | 86 - 195 | 50 - 238 | 82 - 302 | 74 - 291 | 152 - 200 |
| Vapor inlet Reynolds number | 477 - 50,000 | 1670 - 39,200 | 706 - 36,096 | 833 - 43,159 | 808 - 40,000 | 700 - 36,000 |
| Mass flow rate, lb/min | 1.09 - 3.12 | 1.41 - 2.91 | 1.12 - 2.40 | 1.18 - 2.36 | 1.05 - 2.36 | 1.64 - 2.14 |
| Heat rejection rate per unit area$\times 10^{-4}$, Btu/(hr)(sq ft) | 1.26 - 3.59 | 2.00 - 4.14 | 1.04 - 3.22 | 1.35 - 3.47 | 1.21 - 2.80 | 1.89 - 2.46 |
| Outlet quality | 0.0 | 0.0 | 0.0 | 0.0 | 0.0 | 0.0 |
| Remarks | Nonwetting | Nonwetting | Nonwetting | Nonwetting | Wetting | Wetting |

[a]Composition, cobalt - 20 chromium - 15 tungsten - 10 nickel - 1.5 manganese - 0.1 carbon.

TABLE II. - EXPERIMENTAL DATA

(a) Series A

| Run | Flow rate, lb/min | Distance from tube inlet, in. | | | | | | | Condensing length, in. |
|---|---|---|---|---|---|---|---|---|---|
| | | 0 | 18.0 | 36.0 | 54.0 | 72.0 | 90.0 | 102.0 | |
| | | Pressure, mm Hg abs | | | | | | | |
| A-1 | 1.48 | 933 | 910 | 880 | 859 | 856 | 870 | 864 | 94 |
| A-2 | 1.48 | 936 | 906 | 877 | 856 | 848 | 863 | 859 | ↓ |
| A-3 | 1.59 | 999 | 976 | 948 | 930 | 925 | 943 | 939 | |
| A-4 | 1.57 | 993 | 971 | 942 | 923 | 925 | 935 | 931 | |
| A-5 | 1.88 | 900 | 857 | 811 | 785 | 775 | 784 | 780 | ↓ |
| A-6 | 1.92 | 895 | 855 | 812 | 790 | 783 | 790 | 789 | 94 |
| A-7 | 2.52 | 916 | 890 | 802 | 776 | 757 | 794 | 872 | ↓ |
| A-8 | 3.12 | 1546 | 1496 | 1434 | 1409 | 1410 | 1429 | 1522 | |
| A-9 | 3.00 | 1384 | 1333 | 1267 | 1241 | 1237 | 1269 | 1319 | |
| A-10 | 3.00 | 1466 | 1386 | 1317 | 1293 | 1291 | 1311 | 1377 | ↓ |
| A-11 | 1.77 | 639 | 581 | 525 | 504 | 506 | 526 | 569 | 94 |
| A-12 | 1.74 | 648 | 584 | 528 | 505 | 505 | 527 | 549 | ↓ |
| A-13 | 1.92 | 796 | 761 | 715 | 694 | 694 | 711 | 760 | |
| A-14 | 1.85 | 826 | 774 | 728 | 708 | 708 | 736 | 742 | |
| A-15 | 1.82 | 1536 | 1492 | 1467 | 1452 | 1449 | 1464 | 1495 | ↓ |
| A-16 | 1.83 | 1608 | 1560 | 1536 | 1522 | 1522 | 1522 | 1566 | 94 |
| A-17 | 2.13 | 932 | 877 | 829 | 807 | 802 | 807 | 824 | ↓ |
| A-18 | 2.04 | 818 | 752 | 697 | 675 | 670 | 685 | 696 | |
| A-19 | 2.00 | 1034 | 987 | 947 | 931 | 929 | 929 | 950 | |
| A-20 | 1.96 | 1026 | 982 | 939 | 927 | 924 | 934 | 940 | ↓ |
| A-21 | 2.26 | 1134 | 1081 | 1030 | 1010 | 1007 | 1020 | 1033 | 94 |
| A-22 | 2.26 | 1106 | 1054 | 1005 | 986 | 984 | 996 | 1007 | ↓ |
| A-23 | 2.13 | 854 | 779 | 716 | 689 | 688 | 708 | 730 | |
| A-24 | 2.15 | 828 | 758 | 696 | 669 | 669 | 686 | 707 | |
| A-25 | 2.08 | 996 | 962 | 908 | 881 | 882 | 896 | 919 | ↓ |
| A-26 | 2.08 | 1030 | 974 | 929 | 909 | 905 | 919 | 937 | 94 |
| A-27 | 1.28 | 927 | 900 | 874 | 860 | 855 | 860 | 860 | ↓ |
| A-28 | 1.27 | 914 | 887 | 865 | 851 | 848 | 852 | 852 | |
| A-29 | 1.37 | 719 | 678 | 640 | 620 | 617 | 615 | 618 | |
| A-30 | 1.33 | 645 | 606 | 572 | 555 | 551 | 556 | 555 | ↓ |
| A-31 | 1.31 | 442 | 378 | 317 | 284 | 283 | 287 | 299 | 94 |
| A-32 | 1.31 | 432 | 361 | 300 | 271 | 270 | 287 | 300 | ↓ |
| A-33 | 2.20 | 1404 | 1360 | 1322 | 1300 | 1295 | 1302 | 1308 | |
| A-34 | 2.18 | 1354 | 1311 | 1272 | 1250 | 1246 | 1256 | 1267 | |
| A-37 | 1.11 | 596 | 568 | 543 | 529 | 526 | 531 | 537 | ↓ |
| A-38 | 1.09 | 590 | 560 | 537 | 521 | 520 | 527 | 543 | 94 |
| A-39 | 1.24 | 551 | 506 | 468 | 453 | 453 | 463 | 471 | ↓ |
| A-40 | 1.23 | 519 | 476 | 438 | 422 | 422 | 430 | 440 | |
| A-41 | 1.28 | 430 | 365 | 303 | 276 | 276 | 293 | 307 | |
| A-42 | 1.29 | 411 | 345 | 278 | 246 | 246 | 262 | 273 | ↓ |
| A-43 | 2.42 | 1549 | 1502 | 1457 | 1433 | 1428 | 1430 | 1429 | 94 |
| A-44 | 2.40 | 1559 | 1512 | 1469 | 1445 | 1443 | 1448 | 1448 | ↓ |
| A-45 | 1.91 | 1263 | 1220 | 1184 | 1158 | 1160 | 1163 | 1189 | |
| A-46 | 1.87 | 1267 | 1224 | 1191 | 1175 | 1176 | 1188 | 1195 | ↓ |

TABLE II. - Continued. EXPERIMENTAL DATA

(b) Series D

| Run | Flow rate, lb/min | Distance from tube inlet, in. | | | | | | | Condensing length, in. |
|---|---|---|---|---|---|---|---|---|---|
| | | 0 | 14.5 | 29.0 | 43.5 | 58.0 | 72.5 | 87.0 | |
| | | Pressure, mm Hg abs | | | | | | | |
| D-1 | 1.53 | 1369 | 1351 | 1336 | 1325 | 1311 | 1316 | 1318 | 82 |
| D-2 | 1.53 | 1343 | 1335 | 1324 | 1291 | 1298 | 1302 | 1304 | ↓ |
| D-3 | 1.31 | 1248 | 1242 | 1235 | 1222 | 1208 | 1213 | 1205 | ↓ |
| D-4 | 1.31 | 1255 | 1245 | 1237 | 1227 | 1218 | 1220 | 1212 | ↓ |
| D-5 | 2.00 | 1208 | 1189 | 1187 | 1138 | 1113 | 1107 | 1132 | ↓ |
| D-6 | 1.99 | 1231 | 1200 | 1170 | 1150 | 1120 | 1107 | 1114 | 82 |
| D-7 | 2.34 | 1646 | 1617 | 1606 | 1587 | 1558 | 1575 | 1614 | ↓ |
| D-8 | 2.36 | 1536 | 1511 | 1495 | 1472 | 1446 | 1436 | 1476 | ↓ |
| D-9 | 2.05 | 811 | 761 | 745 | 711 | 692 | 682 | 769 | ↓ |
| D-10 | 2.06 | 831 | 793 | 772 | 739 | 724 | 727 | 799 | ↓ |
| D-11 | 1.35 | 801 | 781 | 768 | 753 | 745 | 745 | 779 | 82 |
| D-12 | 1.30 | 794 | 778 | 768 | 745 | 742 | 732 | 755 | ↓ |
| D-13 | 1.19 | 1567 | 1564 | 1559 | 1554 | 1552 | 1547 | 1531 | ↓ |
| D-14 | 1.20 | 1590 | 1584 | 1576 | 1574 | 1574 | 1571 | 1569 | ↓ |
| D-15 | 1.98 | 1546 | 1536 | 1519 | 1509 | 1506 | 1489 | 1493 | ↓ |
| D-16 | 2.00 | 1546 | 1536 | 1521 | 1511 | 1505 | 1494 | 1511 | 82 |
| D-17 | 1.41 | 812 | 795 | 779 | 761 | 760 | 756 | 781 | ↓ |
| D-18 | 1.41 | 800 | 790 | 775 | 757 | 757 | 754 | 780 | ↓ |
| D-19 | 2.09 | 810 | 779 | 754 | 721 | 712 | 710 | 784 | ↓ |
| D-20 | 2.12 | 815 | 787 | 760 | 725 | 715 | 708 | 788 | ↓ |
| D-21 | 2.58 | 1552 | 1527 | 1505 | 1485 | 1470 | 1464 | 1517 | 82 |
| D-22 | 2.57 | 1538 | 1510 | 1487 | 1467 | 1452 | 1445 | 1498 | ↓ |
| D-23 | 2.95 | 1549 | 1517 | 1494 | 1468 | 1448 | 1442 | 1516 | ↓ |
| D-24 | 2.91 | 1552 | 1520 | 1496 | 1470 | 1454 | 1449 | 1525 | ↓ |
| D-25 | 2.74 | 1064 | 1016 | 984 | 942 | 914 | 919 | 1051 | ↓ |
| D-26 | 2.46 | 790 | 739 | 698 | 642 | 593 | 583 | 735 | 82 |
| D-27 | 2.50 | 817 | 771 | 730 | 678 | 635 | 625 | 755 | 82 |
| D-28 | 2.23 | 781 | 746 | 715 | 682 | 671 | 700 | --- | 72 |
| D-29 | 2.22 | 788 | 754 | 725 | 694 | 676 | 702 | --- | 72 |
| D-30 | 1.72 | 777 | 760 | 757 | 755 | 715 | --- | --- | 48 |
| D-31 | 1.67 | 771 | 757 | 754 | 752 | 759 | --- | --- | 48 |

TABLE II. - Continued. EXPERIMENTAL DATA

(c) Series E

| Run | Flow rate, lb/min | Distance from tube inlet, in. | | | | | | | | Condensing length, in. |
|---|---|---|---|---|---|---|---|---|---|---|
| | | 0 | 14.5 | 29.0 | 43.5 | 58.0 | 72.5 | 87.0 | 101.5 | |
| | | Pressure, mm Hg abs | | | | | | | | |
| E-1 | 1.23 | 594 | 589 | 582 | 574 | 574 | 568 | 572 | 564 | 94 |
| E-2 | 1.26 | 582 | 580 | 571 | 563 | 563 | 557 | 560 | 552 | 94 |
| E-3 | 1.20 | 597 | 595 | 602 | 592 | 587 | 582 | 587 | 587 | 72 |
| E-4 | 1.16 | 592 | 594 | 594 | 579 | 589 | 584 | 589 | 589 | 72 |
| E-5 | 1.34 | 607 | 617 | 621 | 620 | 616 | 616 | 611 | 606 | 48 |
| E-6 | 1.34 | 643 | 648 | 650 | 648 | 643 | 646 | 647 | 646 | 48 |
| E-7 | 1.12 | 1057 | 1055 | 1053 | 1043 | 1040 | 1037 | 1033 | 1033 | 94 |
| E-8 | 1.12 | 1047 | 1045 | 1042 | 1040 | 1041 | 1039 | 1038 | 1033 | 94 |
| E-9 | 1.92 | 600 | 590 | 577 | 560 | 558 | 556 | 544 | 536 | 94 |
| E-10 | 1.88 | 609 | 605 | 596 | 586 | 585 | 579 | 587 | 580 | 94 |
| E-11 | 1.93 | 613 | 607 | 593 | 576 | 572 | 565 | 566 | 560 | 94 |
| E-12 | 1.96 | 600 | 594 | 581 | 564 | 558 | 551 | 556 | 550 | 94 |
| E-13 | 1.97 | 593 | 589 | 583 | 578 | 584 | 579 | 579 | 578 | 72 |
| E-14 | 1.97 | 591 | 589 | 588 | 572 | 585 | 580 | 580 | 579 | 72 |
| E-15 | 2.38 | 607 | 603 | 583 | 554 | 550 | 540 | 542 | 537 | 94 |
| E-16 | 2.40 | 597 | 601 | 604 | 559 | 553 | 545 | 549 | 540 | 94 |
| E-17 | 2.25 | 1042 | 1035 | 1034 | 1017 | 1014 | 1008 | 1015 | 1010 | 94 |
| E-18 | 2.38 | 1062 | 1056 | 1043 | 1029 | 1026 | 1021 | 1032 | 1027 | 94 |
| E-19 | 1.20 | 1561 | 1571 | 1570 | 1564 | 1564 | 1563 | 1560 | 1554 | 95 |
| E-20 | 1.30 | 1535 | 1541 | 1541 | 1537 | 1537 | 1539 | 1537 | 1532 | 95 |
| E-21 | 1.97 | 1057 | 1057 | 1054 | 1042 | 1042 | 1037 | 1036 | 1030 | 95 |
| E-22 | 2.01 | 1056 | 1049 | 1042 | 1030 | 1030 | 1029 | 1026 | 1017 | 95 |
| E-23 | 1.35 | 1040 | 1040 | 1039 | 1036 | 1036 | 1031 | 1026 | 1024 | 72 |
| E-24 | 1.34 | 1042 | 1041 | 1041 | 1036 | 1036 | 1036 | 1023 | 1021 | 72 |
| E-25 | 1.25 | 1059 | 1056 | 1054 | 1045 | 1045 | 1046 | 1046 | 1053 | 53 |
| E-26 | 1.23 | 1042 | 1041 | 1039 | 1030 | 1027 | 1028 | 1028 | 1031 | 53 |
| E-27 | 1.20 | 1531 | 1525 | 1523 | 1516 | 1521 | 1523 | 1525 | 1525 | 53 |
| E-28 | 1.18 | 1536 | 1538 | 1538 | 1534 | 1536 | 1536 | 1539 | 1541 | 53 |
| E-29 | 1.88 | 1048 | 1045 | 1043 | 1035 | 1037 | 1030 | 1031 | 1031 | 72 |
| E-30 | 1.85 | 1043 | 1042 | 1041 | 1032 | 1035 | 1033 | 1027 | 1027 | 72 |
| E-31 | 1.99 | 1051 | 1049 | 1047 | 1038 | 1043 | 1035 | 1034 | 1035 | 72 |
| E-32 | 1.94 | 1053 | 1050 | 1050 | 1042 | 1046 | 1042 | 1042 | 1042 | 72 |
| E-33 | 1.78 | 1564 | 1568 | 1568 | 1566 | 1564 | 1572 | 1571 | 1571 | 53 |
| E-34 | 1.75 | 1567 | 1565 | 1563 | 1557 | 1556 | 1555 | 1557 | 1557 | 53 |
| E-35 | 1.75 | 1550 | 1550 | 1557 | 1551 | 1554 | 1554 | 1561 | 1561 | 53 |
| E-36 | 1.73 | 1564 | 1559 | 1554 | 1555 | 1555 | 1548 | 1559 | 1550 | 53 |
| E-37 | 1.94 | 1062 | 1062 | 1062 | 1062 | 1057 | 1058 | 1059 | 1060 | 53 |
| E-38 | 1.96 | 1067 | 1070 | 1071 | 1067 | 1062 | 1065 | 1068 | 1064 | 53 |
| E-39 | 1.72 | 1563 | 1561 | 1555 | 1548 | 1548 | 1541 | 1541 | 1540 | 94 |
| E-40 | 1.77 | 1569 | 1569 | 1564 | 1552 | 1551 | 1546 | 1551 | 1551 | 94 |
| E-41 | 2.10 | 1520 | 1516 | 1496 | 1491 | 1500 | 1493 | 1486 | 1486 | 94 |
| E-42 | 2.04 | 1525 | 1519 | 1517 | 1510 | 1513 | 1512 | 1505 | 1490 | 94 |
| E-43 | 2.26 | 1065 | 1068 | 1058 | 1052 | 1059 | 1059 | 1054 | 1044 | 72 |
| E-44 | 2.24 | 1070 | 1073 | 1067 | 1055 | 1065 | 1062 | 1065 | 1065 | 72 |
| E-45 | 1.166 | 606 | 603 | 591 | 583 | 583 | 581 | 581 | 580 | 94 |
| E-46 | 1.158 | 601 | 592 | 579 | 573 | 573 | 573 | 575 | 572 | 94 |
| E-47 | 1.94 | 1040 | 1042 | 1040 | 1029 | 1023 | 1026 | 1030 | 1021 | 53 |
| E-48 | 1.885 | 1053 | 1052 | 1047 | 1044 | 1037 | 1042 | 1051 | 1052 | 53 |
| E-49 | 1.758 | 1541 | 1535 | 1526 | 1523 | 1523 | 1519 | 1521 | 1516 | 94 |
| E-50 | 1.700 | 1546 | 1546 | 1538 | 1531 | 1531 | 1525 | 1524 | 1516 | 94 |
| E-51 | 1.692 | 1554 | 1547 | 1542 | 1532 | 1532 | 1529 | 1529 | 1527 | 94 |
| E-52 | 1.70 | 1556 | 1554 | 1552 | 1549 | 1552 | 1554 | 1542 | 1539 | 94 |

TABLE II. - Continued. EXPERIMENTAL DATA

(d) Series F

| Run | Flow rate, lb/min | Distance from tube inlet, in. | | | | | | | | Condensing length, in. |
|---|---|---|---|---|---|---|---|---|---|---|
| | | 0 | 14.5 | 29.0 | 43.5 | 58.0 | 72.5 | 87.0 | 101.5 | |
| | | Pressure, mm Hg abs | | | | | | | | |
| F-1 | 1.70 | 941 | 897 | 865 | 844 | 815 | 815 | 817 | 821 | 94 |
| F-2 | 1.70 | 918 | 871 | 838 | 818 | 781 | 844 | 847 | 855 | ↓ |
| F-3 | 2.36 | 744 | 646 | 551 | 463 | 369 | 344 | 344 | 342 | |
| F-4 | 2.36 | 748 | 650 | 553 | 458 | 378 | 350 | 353 | 354 | |
| F-5 | 2.18 | 877 | 795 | 717 | 660 | 598 | 586 | 593 | 602 | ↓ |
| F-6 | 2.18 | 867 | 785 | 723 | 663 | 613 | 593 | 598 | 608 | 94 |
| F-7 | 2.21 | 981 | 916 | 853 | 806 | 765 | 753 | 764 | 772 | 94 |
| F-8 | 2.21 | 967 | 909 | 847 | 802 | 763 | 757 | 764 | 769 | 94 |
| F-9 | 1.92 | 1344 | 1308 | 1287 | 1275 | 1265 | 1271 | 1276 | 1279 | 72 |
| F-10 | 1.92 | 1341 | 1309 | 1289 | 1279 | 1259 | 1265 | 1275 | 1270 | 72 |
| F-11 | 1.21 | 974 | 969 | 957 | 946 | 936 | 935 | 936 | 930 | 94 |
| F-12 | 1.21 | 972 | 966 | 956 | 944 | 934 | 934 | 933 | 927 | 94 |
| F-13 | 1.27 | 963 | 942 | 916 | 910 | 923 | 921 | 922 | 922 | 72 |
| F-14 | 1.27 | 964 | 941 | 915 | 910 | 921 | 920 | 921 | 921 | 72 |
| F-15 | 1.24 | 966 | 954 | 950 | 948 | 944 | 945 | 945 | 946 | 53 |
| F-16 | 1.24 | 966 | 956 | 952 | 952 | 949 | 950 | 950 | 950 | 53 |
| F-17 | 1.69 | 967 | 930 | 906 | 894 | 884 | 887 | 883 | 884 | 72 |
| F-18 | 1.69 | 987 | 942 | 914 | 900 | 885 | 886 | 886 | 888 | 72 |
| F-19 | 1.83 | 968 | 930 | 904 | 892 | 881 | 880 | 880 | 880 | 72 |
| F-20 | 1.83 | 961 | 921 | 897 | 879 | 874 | 874 | 879 | 876 | 72 |
| F-21 | 1.76 | 1569 | 1548 | 1535 | 1529 | 1519 | 1515 | 1524 | 1524 | 72 |
| F-22 | 1.76 | 1565 | 1541 | 1527 | 1516 | 1509 | 1509 | 1509 | 1509 | ↓ |
| F-23 | 1.78 | 1555 | 1524 | 1515 | 1505 | 1502 | 1498 | 1498 | 1498 | |
| F-24 | 1.78 | 1571 | 1543 | 1533 | 1519 | 1511 | 1510 | 1510 | 1505 | |
| F-25 | 2.30 | 975 | 898 | 830 | 778 | 715 | 701 | 704 | 706 | ↓ |
| F-26 | 2.30 | 965 | 887 | 805 | 752 | 687 | 673 | 680 | 676 | 72 |
| F-27 | 1.19 | 616 | 585 | 570 | 544 | 535 | 533 | 548 | 541 | 94 |
| F-28 | 1.19 | 624 | 598 | 580 | 555 | 544 | 537 | 549 | 540 | 94 |
| F-29 | 1.18 | 968 | 953 | 938 | 928 | 916 | 916 | 919 | 911 | 94 |
| F-30 | 1.18 | 970 | 954 | 940 | 927 | 917 | 916 | 917 | 911 | 94 |
| F-31 | 1.26 | 1527 | 1514 | 1502 | 1491 | 1482 | 1492 | 1492 | 1486 | 94 |
| F-32 | 1.26 | 1529 | 1515 | 1502 | 1491 | 1481 | 1481 | 1480 | 1474 | 94 |
| F-33 | 1.76 | 989 | 941 | 903 | 881 | 846 | 842 | 846 | 842 | 94 |
| F-34 | 1.76 | 994 | 944 | 910 | 884 | 856 | 853 | 857 | 850 | 94 |
| F-35 | 1.96 | 975 | 926 | 898 | 879 | 872 | 871 | 877 | 872 | 72 |
| F-36 | 1.96 | 976 | 928 | 897 | 882 | 873 | 874 | 877 | 873 | 72 |
| F-37 | 1.69 | 1520 | 1497 | 1477 | 1464 | 1443 | 1442 | 1443 | 1435 | 94 |
| F-38 | 1.69 | 1520 | 1504 | 1484 | 1467 | 1448 | 1444 | 1445 | 1437 | 94 |
| F-39 | 2.08 | 635 | 533 | 426 | 320 | 198 | 128 | 128 | 154 | 94 |
| F-40 | 2.08 | 636 | 539 | 434 | 331 | 202 | 125 | 122 | 137 | 94 |
| F-42 | 1.32 | 1557 | 1546 | 1538 | 1531 | 1530 | 1532 | 1532 | 1530 | 53 |
| F-43 | 1.84 | 785 | 734 | 697 | 675 | 663 | 664 | 669 | 667 | 72 |
| F-44 | 1.84 | 797 | 746 | 706 | 583 | 570 | 565 | 566 | 561 | 72 |

TABLE II. - Continued. EXPERIMENTAL DATA

(e) Series G

| Run | Flow rate, lb/min | Distance from tube inlet, in. | | | | | | | | Condensing length, in. |
|---|---|---|---|---|---|---|---|---|---|---|
| | | 0 | 14.5 | 29.0 | 43.5 | 58.0 | 72.5 | 87.0 | 101.5 | |
| | | Pressure, mm Hg abs | | | | | | | | |
| G-1 | 2.00 | 1048 | 1030 | 1001 | ---- | 967 | 976 | ---- | ---- | 93 |
| G-2 | 2.00 | 1014 | 972 | 936 | ---- | 905 | 892 | 902 | 904 | 93 |
| G-3 | 2.00 | 1026 | 978 | 935 | 909 | 886 | 891 | 886 | 889 | 93 |
| G-4 | 1.84 | 1028 | 977 | 949 | ---- | 885 | 894 | 895 | 895 | 94 |
| G-5 | 1.84 | 1030 | 988 | 953 | ---- | 890 | 908 | 898 | ---- | 94 |
| G-6 | 1.84 | 1049 | 1009 | 969 | ---- | 927 | 924 | 932 | 931 | 94 |
| G-7 | 2.02 | 996 | 937 | 909 | 882 | 856 | 853 | 856 | 856 | 94 |
| G-8 | 2.02 | 998 | 944 | 906 | 880 | 851 | 850 | 856 | 856 | 94 |
| G-9 | 1.18 | 960 | 941 | 936 | 942 | 931 | 932 | 934 | 929 | 72 |
| G-10 | 1.18 | 958 | 941 | 933 | 932 | 925 | 930 | 933 | 926 | 72 |
| G-11 | 1.18 | 956 | 948 | 946 | 943 | 933 | 942 | 943 | 938 | 72 |
| G-12 | 1.13 | 960 | 948 | 948 | 958 | 950 | 954 | 952 | 947 | 53 |
| G-13 | 1.13 | 959 | 944 | 944 | 955 | 947 | 950 | 946 | 942 | 53 |
| G-14 | 1.19 | 940 | 923 | 922 | 927 | 928 | 932 | 930 | 926 | 53 |
| G-15 | 1.19 | 936 | 916 | 914 | 917 | 917 | 922 | 921 | 912 | 53 |
| G-16 | 1.05 | 910 | 979 | 966 | 953 | 933 | 940 | 952 | 983 | 94 |
| G-17 | 1.05 | 570 | 531 | 518 | 509 | 497 | 497 | 506 | 534 | 94 |
| G-18 | 1.38 | 550 | 504 | 454 | 432 | 417 | 416 | 417 | 468 | 94 |
| G-19 | 1.38 | 548 | 520 | 458 | 428 | 408 | 412 | 413 | 470 | 94 |
| G-20 | 1.25 | 995 | 975 | 965 | 956 | 954 | 953 | 952 | 959 | 94 |
| G-21 | 1.25 | 996 | 975 | 963 | 951 | 948 | 948 | 948 | 956 | 94 |
| G-22 | 1.31 | 974 | 944 | 937 | 938 | 934 | 941 | 941 | 957 | 72 |
| G-23 | 1.31 | 974 | 949 | 939 | 937 | 934 | 940 | 940 | 958 | 72 |
| G-24 | 1.31 | 980 | 965 | 961 | 963 | 961 | 971 | 971 | 977 | 53 |
| G-25 | 1.31 | 982 | 968 | 970 | 967 | 974 | 974 | 973 | 980 | 53 |
| G-26 | 1.66 | 991 | 953 | 917 | 899 | 884 | 883 | 894 | 893 | 94 |
| G-27 | 1.66 | 990 | 929 | 914 | 897 | 884 | 884 | 884 | 887 | 94 |
| G-28 | 1.22 | 1566 | 1553 | ---- | 1541 | 1537 | 1534 | 1535 | 1536 | 94 |
| G-29 | 1.22 | 1562 | 1543 | ---- | 1533 | 1533 | 1533 | 1532 | 1533 | 94 |
| G-30 | 1.22 | 1500 | 1474 | 1502 | 1500 | 1508 | 1515 | 1514 | 1513 | 53 |
| G-31 | 1.22 | 1517 | 1489 | 1511 | 1509 | 1515 | 1512 | 1520 | 1517 | 53 |
| G-32 | 1.77 | 975 | 933 | 917 | 908 | 908 | 916 | 915 | 911 | 72 |
| G-33 | 1.77 | 973 | 929 | 912 | 901 | 899 | 911 | 910 | 908 | 72 |
| G-34 | 1.82 | 1149 | 1207 | 1170 | 1159 | 1148 | 1144 | 1149 | 1149 | 74 |
| G-35 | 1.82 | 1145 | 1196 | 1167 | 1157 | 1142 | 1138 | 1144 | 1145 | 74 |
| G-36 | 2.07 | 1023 | 1184 | 1117 | 1078 | 1043 | 1023 | 1019 | 1023 | 93 |
| G-37 | 2.07 | 1023 | 1177 | 1107 | 1069 | 1039 | 1020 | 1020 | 1023 | 93 |
| G-38 | 2.29 | 968 | 888 | 831 | 792 | 761 | 761 | 761 | 768 | 93 |
| G-39 | 2.29 | 968 | 893 | 836 | 787 | 758 | 758 | 763 | 765 | 93 |
| G-40 | 1.70 | 1544 | 1515 | 1500 | 1489 | 1485 | 1482 | 1481 | 1482 | 93 |
| G-41 | 1.70 | 1537 | 1507 | 1486 | 1474 | 1469 | 1468 | 1468 | 1469 | 93 |
| G-42 | 1.79 | 1572 | 1540 | 1521 | 1507 | 1498 | 1496 | 1496 | 1496 | 94 |
| G-43 | 1.79 | 1575 | 1543 | 1523 | 1510 | 1502 | 1501 | 1503 | 1505 | 94 |
| G-44 | 1.65 | 1557 | 1533 | 1524 | 1520 | 1516 | 1512 | 1514 | 1513 | 72 |
| G-45 | 1.65 | 1542 | 1516 | 1506 | 1500 | 1497 | 1501 | 1502 | 1500 | 72 |
| G-46 | 1.86 | 1532 | 1503 | 1491 | 1486 | 1483 | 1488 | 1489 | 1485 | 72 |
| G-47 | 1.86 | 1532 | 1504 | 1491 | 1485 | 1484 | 1490 | 1491 | 1488 | 72 |
| G-48 | 1.84 | 582 | 491 | 410 | 348 | 297 | 297 | 301 | 325 | 94 |
| G-49 | 1.84 | 578 | 494 | 411 | 344 | 293 | 293 | 297 | 320 | 94 |
| G-50 | 1.15 | 1548 | 1537 | 1534 | 1533 | 1533 | 1534 | 1534 | 1532 | 72 |
| G-51 | 1.15 | 1566 | 1554 | 1550 | 1548 | 1547 | 1548 | 1547 | 1544 | 72 |
| G-52 | 2.36 | 1547 | 1482 | 1437 | 1411 | 1390 | 1386 | 1390 | 1389 | 94 |
| G-53 | 2.36 | 1543 | 1483 | 1437 | 1413 | 1390 | 1386 | 1389 | 1389 | 94 |

TABLE II. - Concluded. EXPERIMENTAL DATA

(f) Series W

| Run | Flow rate, lb/min | Distance from tube inlet, in. | | | | | | | Condensing length, in. |
|---|---|---|---|---|---|---|---|---|---|
| | | 0 | 18.0 | 36.0 | 54.0 | 72.0 | 90.0 | 102.0 | |
| | | Pressure, mm Hg abs | | | | | | | |
| W-1 | 1.64 | 1042 | 1000 | 968 | 951 | 948 | 948 | 944 | 94 |
| W-2 | 1.72 | 1030 | 988 | 967 | 958 | 953 | 945 | 945 | ↓ |
| W-3 | 1.92 | 1021 | 981 | 959 | 951 | 937 | 939 | 945 | |
| W-4 | 2.11 | 1013 | 967 | 945 | 924 | 919 | 909 | 923 | |
| W-5 | 2.14 | 1030 | 990 | 954 | 937 | 933 | 928 | 931 | |



NASA-Langley, 1964 E-2625

*"The aeronautical and space activities of the United States shall be conducted so as to contribute . . . to the expansion of human knowledge of phenomena in the atmosphere and space. The Administration shall provide for the widest practicable and appropriate dissemination of information concerning its activities and the results thereof."*

—NATIONAL AERONAUTICS AND SPACE ACT OF 1958

# NASA SCIENTIFIC AND TECHNICAL PUBLICATIONS

TECHNICAL REPORTS: Scientific and technical information considered important, complete, and a lasting contribution to existing knowledge.

TECHNICAL NOTES: Information less broad in scope but nevertheless of importance as a contribution to existing knowledge.

TECHNICAL MEMORANDUMS: Information receiving limited distribution because of preliminary data, security classification, or other reasons.

CONTRACTOR REPORTS: Technical information generated in connection with a NASA contract or grant and released under NASA auspices.

TECHNICAL TRANSLATIONS: Information published in a foreign language considered to merit NASA distribution in English.

TECHNICAL REPRINTS: Information derived from NASA activities and initially published in the form of journal articles.

SPECIAL PUBLICATIONS: Information derived from or of value to NASA activities but not necessarily reporting the results of individual NASA-programmed scientific efforts. Publications include conference proceedings, monographs, data compilations, handbooks, sourcebooks, and special bibliographies.

***Details on the availability of these publications may be obtained from:***

**SCIENTIFIC AND TECHNICAL INFORMATION DIVISION**

**NATIONAL AERONAUTICS AND SPACE ADMINISTRATION**

**Washington, D.C. 20546**